Available online at www.sciencedirect.com
ScienceDirect
Journal of Solid State Chemistry 181 (2008) 789–795
JOURNAL OF SOLID STATE CHEMISTRY
www.elsevier.com/locate/jssc

Linear and nonlinear optical susceptibilities for a novel borate oxide $BaBiBO_4$: Theory and experiment

Ali Hussain Reshak[a,b,*], S. Auluck[c], I.V. Kityk[d]

[a]*Institute of Physical Biology, South Bohemia University, Zamek 136, Nove Hrady 37333, Czech Republic*
[b]*Institute of System Biology and Ecology, Academy of Sciences, Nove Hrady 37333, Czech Republic*
[c]*Physics Department, Indian Institute of Technology, Kanpur, UP 208016, India*
[d]*Institute of Physics, J. Dlugosz University of Czestochowa, Al. Armii Krajowej 13/15, Czestochowa, Poland*

Received 26 September 2007; received in revised form 4 January 2008; accepted 7 January 2008
Available online 17 January 2008

Abstract

The linear and nonlinear optical susceptibilities for different tensor components of $BaBiBO_4$ single crystals have been calculated using the full-potential linear augmented plane wave method. The results of these calculations are verified by our measurements of linear and nonlinear optical properties using Nd-YAG laser at fundamental wavelength 1064 nm. The calculated energy gap is in a good agreement with experimental energy gap data obtained by optical absorption. We present results for the imaginary and real parts of the frequency-dependent dielectric constant. The calculated birefringence of $BaBiBO_4$ is positive in agreement with the experimental data. Calculations are reported for the frequency-dependent complex part of second-order nonlinear optical susceptibilities $\chi^{(2)}_{ijk}(\omega)$. The linear and nonlinear optical susceptibilities are scissors corrected to match the value of the energy gap from the local density approximation calculations with the experimental value. The second harmonic generation efficiency of this compound is about five times larger than KDP (KH_2PO_4). It is crucial that we have obtained a large anisotropy of the second-order susceptibilities for three main second-order tensor components $\chi^{(2)}_{zzz}(\omega)$, $\chi^{(2)}_{xxz}(\omega)$, and $\chi^{(2)}_{yyz}(\omega)$ both experimentally and theoretically. The possible origin of the obtained anisotropy is discussed within a framework of the energy band calculations.

Keywords: Electronic structure; Optical properties (linear and nonlinear); SHG; DFT; LDA; FPLAPW

1. Introduction

As a result of their complicated crystal structures borates are among the most interesting and therefore the most extensively studied materials. Since 1962, when the binary phase diagram Bi_2O_3–B_2O_3 were investigated, many methods of obtaining the borate crystals were found and described in detail [1–6]. It was also established that borate crystals, in particular BiB_3O_6, exhibit high nonlinear optical (NLO) susceptibilities [7–10], particularly for second harmonic generation (SHG) and third harmonic generation (THG) applications. Theoretical examinations have shown that anionic groups and chemical bonding structures of boron atoms have a major influence on the nonlinear properties of these crystals [11,12].

With a view of finding new optical materials, $BaBiBO_4$ was synthesized recently [13]. This is principally different compared to other borate crystals due to the presence of two different structural clusters—BO_3 and BiO_5 having substantially different ionicities. Another principal difference of these crystals with respect to other borates consists is the large anisotropy of the chemical bonds due to layered structures. This factor may have both technological interest pertaining to the creation of the optical devices and fundamental interest for theory of linear and NLO susceptibilities for the new synthesized oxide crystals. There is a dearth of a detailed investigation connecting the electronic structure and the measured susceptibilities for the highly anisotropic material. We hope that our work will be useful in this direction.

*Corresponding author at: Institute of Physical Biology, South Bohemia University, Zamek 136, Nove Hrady 37333, Czech Republic. Fax: +420 386 361 390.
E-mail address: maalidph@yahoo.co.uk (A.H. Reshak).

0022-4596/$ - see front matter © 2008 Elsevier Inc. All rights reserved.
doi:10.1016/j.jssc.2008.01.018

The knowledge of the band structure plays a principle role in understanding their physical properties. The considered compound is particularly interesting for its NLO properties, which could be related to the anionic and cationic polyhedral and to find such directions in which these materials may give large optical susceptibilities. Utilizing their anisotropy and there appears a possibility to increase the corresponding optical susceptibilities. Moreover, by inducing changes in the cationic sub-systems one can also vary the transparency and mechanical properties. Thus one requires reliable information about band structure.

In this paper, we report both the measurements and the calculations of linear and NLO susceptibilities. For the theoretical calculation we used the full-potential linear augmented plane wave (FP-LAPW) method and compare the performed calculation with the our experimental data using the Nd-YAG laser at fundamental wavelength 1064 nm, and compare the band structure with X-ray photoelectron parameters [14]. As there are no theoretical calculations of the linear and NLO properties for $BaBiBO_4$ crystal, we report such calculations in this paper and try to find physical origin of the observed anisotropy.

Section 2 describes calculation procedure and experimental technique used for the $BaBiBO_4$ optical parameter evaluations. Section 3 presents principal results of the performed theoretical band energy, optical susceptibility calculations, and their comparison with the experimental data is given with appropriate discussion.

2. Calculation and experimental methodology

2.1. Calculation details

Using X-ray diffraction we found that the $BaBiBO_4$ single crystal belongs to the $Pna2_1$ space group and the parameters of the primitive orthorhombic unit cell with four formula per unit cell, are $a = 8.5822$ Å, $b = 9.6808$ Å, $c = 5.1508$ Å and $Z = 4$. The crystal structure contains parallel chains formed by BO_3 and BiO_5 groups. Chains are directed along [001] direction and separated with rows of Bi^{3+} cations. As seen from Fig. 1, the atomic positions for the $BaBiBO_4$ structure show small but significant deviation from the centro-symmetric group in which the Ba, Bi, B, O1 and O4 atoms would lie on a mirror plane at $z = 0.75$, and the O2 and O3 atoms would become equivalent [13]. Generally the crystalline structure possesses substantial anisotropy with respect to the optical axes z, which is substantially larger compared to other borates.

Our calculations employ the FP-LAPW method as implemented in WIEN2K code [15] based on DFT [16]. A fully relativistic description for the core states, but a scalar-relativistic description, neglecting spin–orbit coupling, for the valence states is used. For structural properties the exchange correlation potential was calculated using the local density approximation (LDA) [17]. In order to achieve energy convergence, the wave functions in the interstitial region were expanded in plane waves with a cutoff $K_{max} = 9/R_{MT}$, where R_{MT} denotes the smallest atomic sphere radius and K_{max} gives the magnitude of the largest K vector in the plane wave expansion. The valence wave functions inside the spheres are expanded up to $l_{max} = 10$ while the charge density was Fourier expanded up to $G_{max} = 14$. Self-consistency is obtained using 200 $\boldsymbol{k}$-points in the irreducible wedge of the irreducible Brillouin zone (IBZ). The BZ integrations are carried out using the tetrahedron method [18,19]. The frequency-dependent linear optical properties are calculated using 500 $\boldsymbol{k}$-points and the NLO properties using 1000 k-points in the IBZ. Both the plane wave cutoff and the number of $\boldsymbol{k}$-points were varied to ensure total energy convergence. The self-consistent calculations are considered to be converged when the total energy of the system is stable to within 10^{-5} Ry.

2.2. Experimental details

Optical absorption spectra were measured by UV–VIS spectrophotometer Ocean Optics with the spectral resolution about 1 nm. The second-order optical susceptibilities were measured by standard method [28] using 10 ns Nd-YAG laser (Carat, Lviv, Ukraine, 2005) with pulse repetition 7 Hz. The Glan prisms were used for

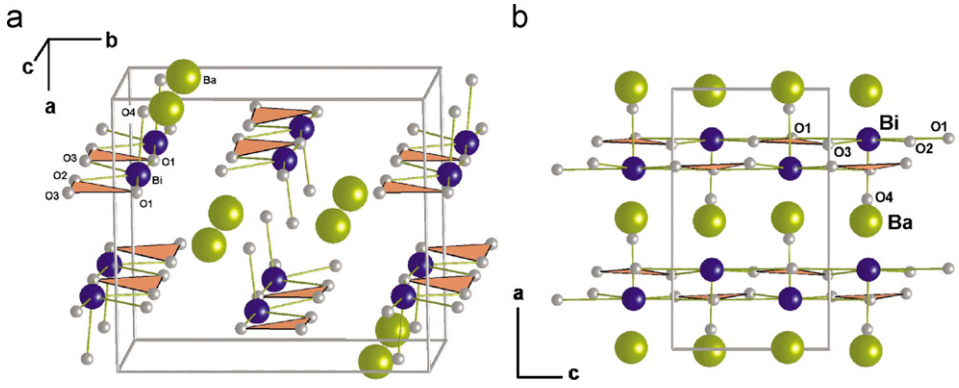

Fig. 1. Projection of the $BiBaBO_4$ crystal structure in (a) along to [001] chains of edge-sharing BO_3 triangles and BiO_5 polyhedra and (b) along [010] direction illustrating the absence of a mirror plane perpendicular to the c axis resulting in the acentric $Pna2_1$ symmetry [13].

definition of the input and output directions to measure the different tensor components of the second-order optical susceptibilities. The green interferometric filter was used to cut the output doubled-frequency signal at 533 nm with respect to the fundamental ones. Detection was performed by fast response photodiodes connected with the GHz oscilloscope (Newport). The crystals were cut in directions that allowed to carry out the measurements for three principal tensor components: $\chi^{(2)}_{zzz}(\omega)$, $\chi^{(2)}_{xxz}(\omega)$, and $\chi^{(2)}_{yyz}(\omega)$. The samples possessed the varied thickness, which allowed obtaining the optimal phase-matching conditions. The setup allows achieving the precision of the second-order susceptibility determination equal to about 0.08 pm/V.

3. Results and discussions

3.1. Electronic energy band structure

The calculated electronic band structure for $BaBiBO_4$ crystal is shown in Fig. 2. The valence band maximum (VBM) is located at Γ while the conduction band minimum (CBM) is located at X resulting in an indirect energy gap of 3.53 eV. The calculated energy gap is smaller than the experimental gap (4.21 eV) as expected from LDA calculation [19]. The band structure can be divided into five groups. The lowest energy group has mainly Bi-*s* and Ba-*p* states origin. The group between −5.5 and −3.5 eV has significant contributions from Bi-*p*/*d*, B-*s*/*p*, Ba-*s* and O-*s* states. The group between −2.5 eV and Fermi energy (E_F) is mainly Bi-*p*/*d*/*f*, B-*p*, O-*p* and Ba-*s*. The conduction band (3.5 up to 8.0 eV) is found to be Bi-*p*/*d*, B-*p*, Ba-*s* and O-*s* states. The electronic structure of the upper valence band arises primarily from the Ba-*p*/*d*, Bi-*p*/*d* and B*s*/*p* interactions. We note that most of the Ba-*d* states are concentrated in the upper conduction band, with negligible contribution to the valence band. Most of the Ba-*p* states are pushed from the conduction bands into valence bands.

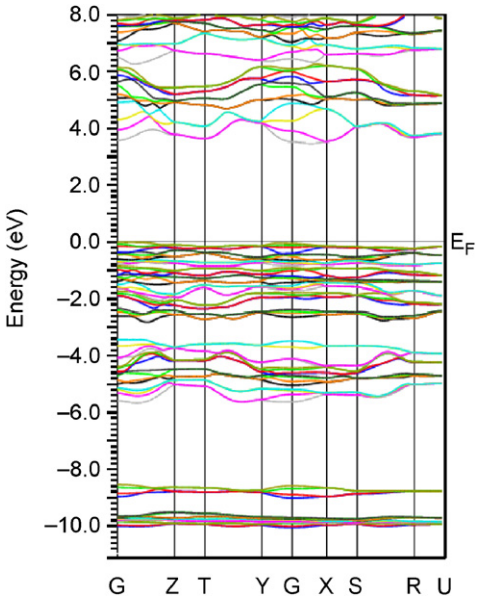

Fig. 2. Calculated electronic energy band structure.

3.2. Linear optical response and birefringence

The orthorhombic symmetry (due to low symmetry) compounds have many non-zero components of the dielectric tensor. We will concentrate on the major components, corresponding to electric field $\vec{E}$ perpendicular and parallel to the *c*-axis. These are $\varepsilon_2^{xx}(\omega)$ and $\varepsilon_2^{zz}(\omega)$ the imaginary parts of the frequency-dependent dielectric function. We have performed calculations of the frequency-dependent dielectric function for these compounds using the expressions given earlier [20,21]. Fig. 3a shows the calculated imaginary parts of the anisotropic frequency-dependent dielectric function $\varepsilon_2^{xx}(\omega)$ and $\varepsilon_2^{zz}(\omega)$. A considerable anisotropy is found between $\varepsilon_2^{xx}(\omega)$ and $\varepsilon_2^{zz}(\omega)$. This may reflect the anisotropy in the directions of the principal chemical bonds (see Fig. 1) and is very sensitive to the ionicity of the cationic sub-system. Half-width broadening is taken to be 0.04 eV following the typical values for the borate crystals. Our optical spectra are scissors corrected [22,23] by 0.68 eV. This value is the difference between the calculated (3.53 eV) and measured (4.21 eV) energy gap.

It is known that spectral peaks in the optical response are caused by the electric-dipole transitions between the valence and conduction bands. Our analysis of $\varepsilon_2^{xx}(\omega)$

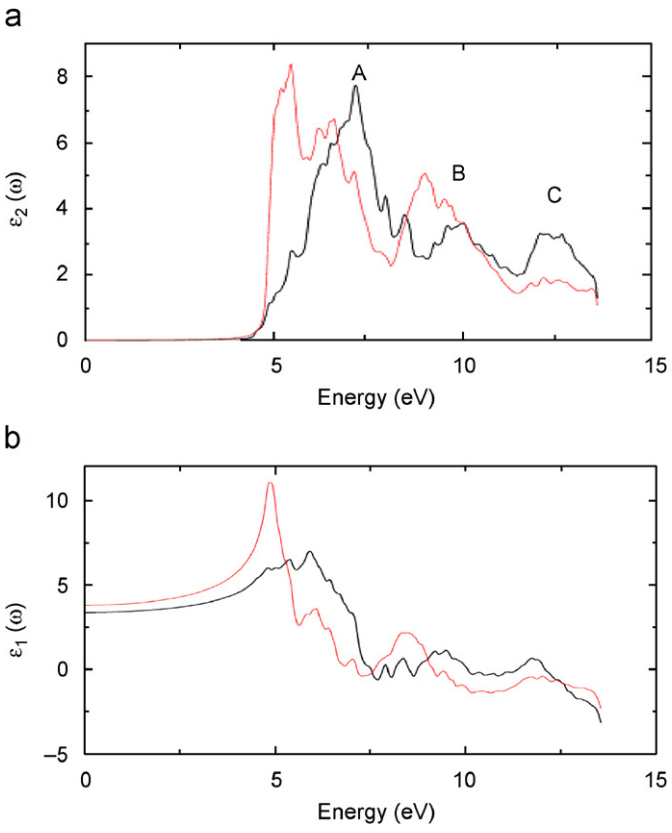

Fig. 3. (a) Calculated $\varepsilon_2^{xx}(\omega)$ (dark curve) and $\varepsilon_2^{zz}(\omega)$ (light curve). (b) Calculated $\varepsilon_1^{xx}(\omega)$ (dark curve) and $\varepsilon_1^{zz}(\omega)$ (light curve).

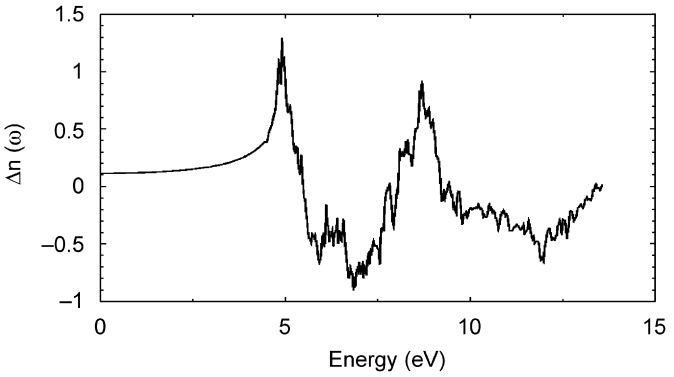

Fig. 4. Calculated $\Delta n(\omega)$.

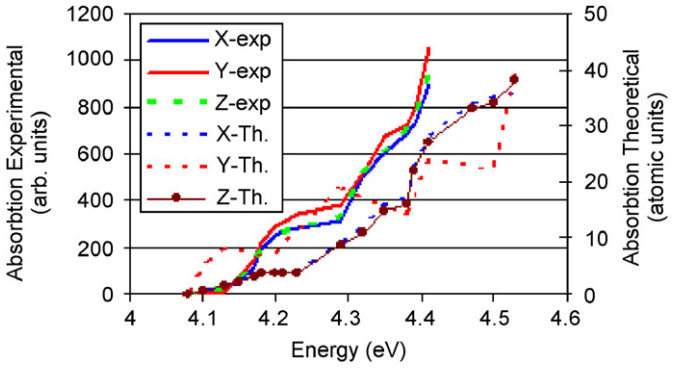

Fig. 5. Absorption spectrum of $BaBiBO_4$ for three polarizations. The direct energy gap is about 290 nm and the energy gap due to the indirect transitions (related to several vacancies and non-stoichiometric defects)—about 296 nm.

and $\varepsilon_2^{zz}(\omega)$ curves shows that the edge of optical absorption for $\varepsilon_2^{xx}(\omega)$ is situated at 4.0 eV, while that for $\varepsilon_2^{zz}(\omega)$ is at 3.8 eV. These points correspond to $\Gamma_v - X_c$ band energy splitting (Fig. 2), which gives the threshold for optical transitions between the top of valence band and bottom of CBM. This is followed by three spectral bands indicated by A, B and C. We note that the first two spectral structures of $\varepsilon_2^{zz}(\omega)$ are shifted towards the lower energy showing considerable anisotropy with respect to $\varepsilon_2^{xx}(\omega)$.

From the imaginary parts of the dielectric functions $\varepsilon_2^{xx}(\omega)$ and $\varepsilon_2^{zz}(\omega)$, the real parts $\varepsilon_1^{xx}(\omega)$ and $\varepsilon_1^{zz}(\omega)$ are calculated by using Kramers–Kronig relations [24]. The results of our calculated $\varepsilon_1^{xx}(0)$ and $\varepsilon_1^{zz}(0)$ spectra are shown in Fig. 3b. The calculated static value of the dielectric functions $\varepsilon_1^{xx}(\omega)$ and $\varepsilon_1^{zz}(\omega)$ are 3.4 and 3.8, respectively.

Generally, this compound shows a considerable anisotropy in the linear optical susceptibilities that favors an important quantity in second-order susceptibility (determining SHG) and optical parametric oscillator (OPO) due to better fulfilling of phase-matching conditions, determined by birefringence. The birefringence is the difference between the extraordinary and ordinary refraction indices, $\Delta n = n_e - n_o$, where in our case n_e is the index of refraction for an electric field oriented along the c-axis and n_o is the index of refraction for an electric field perpendicular to the c-axis.

Fig. 4 shows the spectral behavior of the birefringence $\Delta n(\omega)$ for the $BaBiBO_4$ single crystal. The birefringence is important only in the non-absorbing region (below energy gap). The $\Delta n(\omega)$ spectral dependence shows strong oscillations around zero in the spectral energy range up to 12.5 eV. We have found that the birefringence $\Delta n(0)$ of $BaBiBO_4$ crystal is equal to 0.35 in qualitative agreement with the experimental data 0.24.

Fig. 5 shows the experimentally obtained absorption spectra measured by the Specord 80 M spectrophotometer with a spectral resolution about 1 nm. The data indicate that the absorption edge possess several bends indicating several contributions of the phonon-assisted indirect inter-band transitions and a presence of the non-stoichiometry vacancies. The data show substantial anisotropy in accordance with the performed calculations of the absorption and ε_2, which also confirms the anisotropy in the crystal structure. This anisotropy is attributed to the anisotropy in the energy band structure and the refractive indices. The formation of the spectral plateau at the spectral range about 290 nm is typical for the indirect transitions in the oxide crystals. The anisotropy of the absorption optical spectra is probably caused by specific coordination strength of the bismuth ions. In Fig. 5, we compared both the experimental data and theoretical calculations and found good agreement as far as the trends are concerned. Absolute values are very different because the experimental data are influenced by sample preparation and surface.

3.3. Second harmonic generation

The complex second-order NLO susceptibility tensor $\chi_{ijk}^{(2)}(-2\omega;\omega;\omega)$ has been presented in previous works [25,26]. Subscripts or superscripts i, j and k are Cartesian indices. It has been demonstrated by Aspnes [27] that only virtual-electron transitions (transitions between one valence band state and two conduction band states) gives a significant contribution to the second-order tensor. Hence, we ignore the virtual-hole contribution (transitions between two valence band states and one conduction band state) because it is more than an order of magnitude smaller than the virtual-electron contribution for these compounds. For simplicity we denote $\chi_{ijk}^{(2)}(-2\omega;\omega;\omega)$ by $\chi_{ijk}^{(2)}(\omega)$. For non-centro-symmetric compounds with orthorhombic mmm point group of symmetry, seven independent non-zero tensor components $\chi_{ijk}^{(2)}(\omega)$ exists. Namely, the 131 = 113, 232 = 223, 311, 322 and 333 components (1, 2 and 3 refer to the x, y and z axes, respectively) [28]. These are $\chi_{113}^{(2)}(\omega)$, …, and $\chi_{333}^{(2)}(\omega)$. It is well known that NLO properties are more sensitive to small changes in the band structure than the linear optical properties. This is attributed to the fact that the second harmonic response $\chi_{ijk}^{(2)}(\omega)$ involves 2ω resonance in addition to the usual ω resonance. Both the ω and 2ω resonances can be additionally separated into inter-band and intra-band contributions.

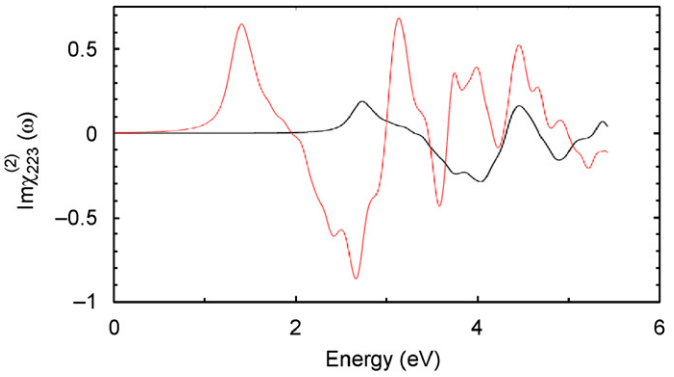

Fig. 6. Calculated $\mathrm{Im}\,\chi^{(2)}_{223}(\omega)$ (dark curve) with scissors correction and (light curve) without scissors correction.

Fig. 6 shows the calculated imaginary part of $\chi^{(2)}_{ijk}(\omega)$ with and without scissors corrections. We see that the scissors correction has a profound effect on magnitude and sign of $\chi^{(2)}_{ijk}(\omega)$. This could be traced to the fact that LDA calculations usually underestimate the energy gaps. A very efficient way to overcome this drawback is to use the scissor correction, which merely makes the calculated energy gap very close to the experimental gap. The calculated imaginary part of the SHG susceptibility $\chi^{(2)}_{ijk}(\omega)$ for all components are shown in Fig. 7. A definite enhancement in the anisotropy on going from linear optical properties to the NLO properties is evident. In Fig. 8, we show the 2ω inter-band and intra-band contributions for the 223 component. We note the opposite signs of the two contributions throughout the measured frequency range. Any anisotropy in the linear optical properties is enhanced in the nonlinear spectra.

One can see that the total SHG response is zero below half the band gap. The 2ω terms start contributing at energies $\sim 1/2E_g$ and the ω terms for energy values above E_g. In the low-energy range ($\leqslant 4$ eV) the SHG optical spectra is dominated by the 2ω contributions. Beyond 4 eV the major contribution is originated from the ω terms. The effective second-order nonlinear coefficient d_{eff} is one of the most important parameters that characterizes the NLO properties of a crystal. The d_{eff} also can be calculated using the second-order nonlinear susceptibility d_{ij} of the crystal. The effective nonlinear coefficient d_{eff} of $BaBiBO_4$ crystal estimated to be five times larger than KDP crystal (KH_2PO_4). We note that $\chi^{(2)}_{223}(\omega)$ is the dominant component (Fig. 7), which shows the largest value of total $\mathrm{Re}\chi^{(2)}_{ijk}(0)$ compared to the other components (Tables 1 and 2).

Unlike the linear optical spectra, the features in the SHG susceptibility are very difficult to identify from the band structure because of the simultaneous presence of resonance 2ω and ω terms. But we can make use of the linear optical spectra to identify the different resonance leading to various features in the SHG spectra. The structures in $\mathrm{Im}\,\chi^{(2)}_{ijk}(\omega)$ between 2.1 and 4.5 eV is mainly due to 2ω resonance. The structure from 4.5 to 5.5 eV is associated

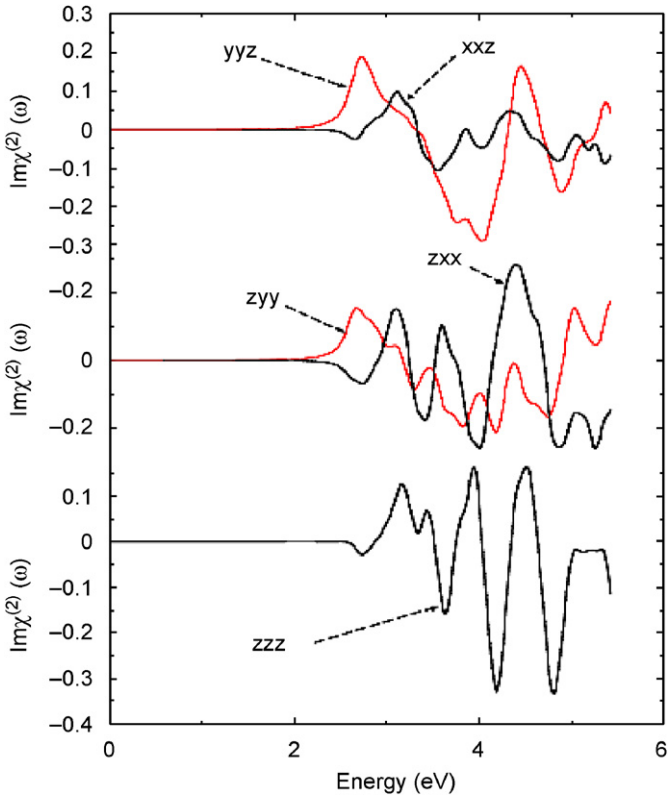

Fig. 7. Upper panel: calculated $\mathrm{Im}\,\chi^{(2)}_{113}(\omega)$ (dark curve) and $\mathrm{Im}\,\chi^{(2)}_{223}(\omega)$ (light curve). Second panel: calculated $\mathrm{Im}\,\chi^{(2)}_{311}(\omega)$(dark curve) and $\mathrm{Im}\,\chi^{(2)}_{322}(\omega)$(light curve). Third panel: calculated $\mathrm{Im}\,\chi^{(2)}_{333}(\omega)$. All $\mathrm{Im}\,\chi^{(2)}(\omega)$ are multiplied by 10^{-7}, in esu units.

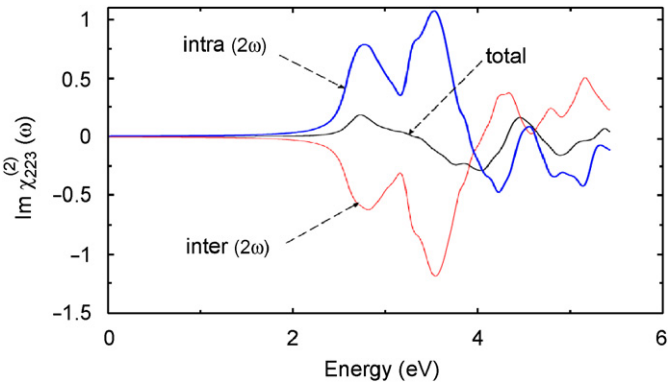

Fig. 8. Calculated $\mathrm{Im}\,\chi^{(2)}_{223}(\omega)$ along with the intra (2ω) and inter (2ω)-band contributions. All $\mathrm{Im}\,\chi^{(2)}(\omega)$ are multiplied by 10^{-7}, in esu units.

with superposition between the ω fundamental resonance and doubled-frequency 2ω resonance. We present the values of $\chi^{(2)}_{ijk}(0)$ for all the components in Table 1.

From an experimental viewpoint, one of the quantities of interest is the magnitude of SHG, we present the absolute values of $\chi^{(2)}_{113}(\omega), \chi^{(2)}_{223}(\omega), \chi^{(2)}_{311}(\omega), \chi^{(2)}_{322}(\omega)$ and $\chi^{(2)}_{333}(\omega)$ in Fig. 9. The first peak for these components are located at $2\omega = 3.4, 2.7, 3.3, 2.6, 3.2$ eV with the peak values of (0.14, 0.18, 0.22, 0.15, 0.13) $\times 10^{-7}$ esu, respectively.

Table 1
Calculated total and intra inter-band of the zero frequency of the real part of the $\mathrm{Re}\chi^{(2)}_{ijk}(\omega)$

Components	*xxz*	*yyz*	*zxx*	*zyy*	*zzz*
$\mathrm{Re}\chi_{ijk}(0)$ total	−0.01	0.02	−0.02	0.025	0.01
$\mathrm{Re}\chi_{ijk}(0)$ inter	−0.13	−0.22	−0.22	−0.4	−0.36
$\mathrm{Re}\chi_{ijk}(0)$ intra	0.12	0.2	0.11	0.3	0.25
Total $\mathrm{Re}\chi_{ijk}(0)$ pm/V	0.4	0.55	−0.45	0.54	0.15

The $\mathrm{Re}\chi^{(2)}_{ijk}(0)$ total, inter, and intra are expressed in units of 1×10^{-7} esu. The total $\mathrm{Re}\chi^{(2)}_{ijk}(0)$ pm/V is expressed in pm/V, in SI units.

Table 2
Principal experimental and theoretically calculated components: position of theoretically calculated first spectral maxima (E_{max}); calculated absolute values of the first spectral maxima (in 10^{-7} esu)—I_{max}; experimentally measured values of the second-order susceptibilities at 1064 nm in pm/V−χ_{exp}

Components	E_{max} (eV)	I_{max} (in 10^{-7} esu)	χ_{exp} (pm/V)	χ_{calc} (pm/V)
xxz	3.4	0.14	0.51	0.4
yyz	2.7	0.18	1.13	0.55
zzz	3.2	0.13	0.13	0.15

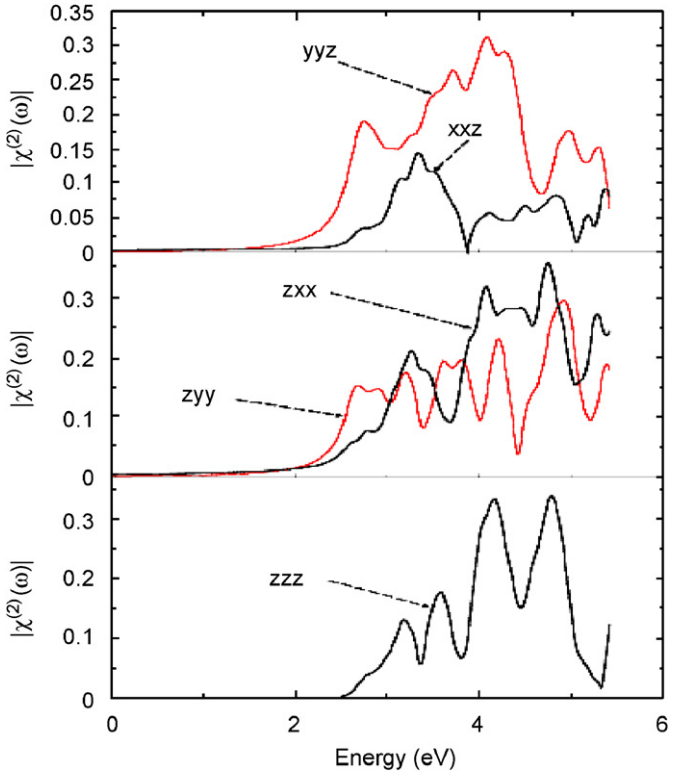

Fig. 9. Calculated absolute values of $\chi^{(2)}_{ijk}(\omega)$ for *xxz*, *yyz*, *zxx*, *zyy*, and *zzz* second-order optical susceptibility components, all $\chi^{(2)}_{ijk}(\omega)$ multiplied by 10^{-7}, in esu units.

To compare the calculated values with the experimental data, in Table 2 we have presented the measured second-order susceptibilities at 1064 nm with the spectral positions of the first oscillator of theoretically calculated values of the corresponding susceptibilities and the values of the corresponding maxima for second-order susceptibility maxima. One can clearly see a good correlation between the theoretically evaluated and experimental data of the susceptibilities. However comparing these data with Table 1, and in Figs. 7 and 8 one can see the importance of inter-band transitions in the energy range 3–5 eV. These transitions are very sensitive to the chemical bond anisotropy and the further search of the crystals with the desired properties the researchers should take into account the bands originated from these transitions. Following Figs. 7 and 8 we can understand why the NLO susceptibilities give substantially larger anisotropy compared to the linear ones. Based on the theoretical calculations the main design strategy should be directed on a search of the cationic sub-systems with the less ionicity with respect to the borate anionic complexes. The principal contribution comes from the intra-layer 2*p*O–2*p*B antibonding anions while the inter-layer gives substantially less contribution.

4. Conclusions

The linear and NLO susceptibilities of nonlinear $BaBiBO_4$ were calculated using FP-LAPW method. The results of these calculations are verified by our measurements of linear and NLO properties using Nd-YAG laser at fundamental wavelength 1064 nm. Comparison with our experimental data shows a sufficiently good agreement and confirms large anisotropy with respect to optical axes *c*. The highest value of the second-order susceptibilities was obtained for the *yyz* second-order susceptibility at 1064 nm fundamental wavelength and the corresponding value for the *zzz* component is almost one order less. These results correlated with the anisotropy in the structure of the investigated crystal. The principal role gives intra-layer 2*p*O–2*p*B antibonding anions and the perpendicular contributions of the ionic components give substantially less contribution. The linear optical susceptibilities show a strong anisotropy that favors an important quantity in SHG and OPO's due to better fulfilling of phase-matching conditions, determined by birefringence. The performed calculations show a possible enhancement of the observed optical susceptibilities by appropriate changes of anisotropy between the intra-layer covalent and inter-layer ionic chemical bonds.

Acknowledgments

The authors would like to thank the Institute Computer Center, for providing the computational facilities. They would also like to thank Prof. Claudia Ambrosch-Draxl, 000 Montan Universität Leoben, 8700 Leoben, Franz-Josef-StraBe 18, Austria, and Dr. Sangeeta Sharma, Institut für Theoretische Physik, Freie Universität Berlin, Arnimallee 14, D-14195 Berlin, Germany. We would like to

thank Prof. J. Barbier, Dept. of Chemistry, McMaster University, Canada, for the kind help by allowing us to use Figure 1 in this article from his published paper [13]. This work was supported from the institutional research concept of the Institute of Physical Biology, UFB (No. MSM6007665808), and the Institute of System Biology and Ecology, ASCR (No. AVOZ60870520).

References

[1] J. Liebertz, Z. Krystallogr 158 (1982) 319;
J. Liebertz, S. Stahr, Z. Kristallogr. 165 (1983) 95.
[2] Z. Weizhuo, H. Huicong, L. Zhiping, Z. Thiande, H. Sukun, T. Dingyuan, Z. Qinglan, Sci. China (Ser. B) 38 (2) (1995).
[3] P. Becker, J. Liebertz, L. Bohaty, J. Cryst. Growth 203 (1999) 149.
[4] A.A. Kaminskii, P. Becker, L. Bohaty, K. Ueda, K. Takaichi, J. Hanuza, M. Maczka, H.J. Eichler, M.A. Gad, Opt. Commun. 206 (2002) 179;
M. Burianek, P. Held, M. Muhlberg, Cryst. Res. Technol. (2002) 179.
[5] M. Burianek, P. Held, M. Muhlberg, Cryst. Res. Technol. 37 (2002) 785.
[6] S. Filatov, Y. Shepelev, R. Bubnova, N. Sennova, A.V. Egorysheva, Y.F. Kargin, J. Solid State Chem. 177 (2004) 515;
H. Hellwig, J. Liebertz, L. Bohaty, Solid State Commun. 109 (4) (1999);
M. Ghotbi, M. Ebrahim-Zadeh, A. Majchrowski, E. Michalski, I.V. Kityk, Opt. Lett. 29 (2004) 2530;
M. Ghotbi, Z. Sun, A. Majchrowski, E. Michalski, I.V. Kityk, Appl. Phys. Lett. 89 (2006) 173124.
[7] A. Brenier, I.V. Kityk, A. Majchrowski, Opt. Commun. 203 (2002) 125;
A. Majchrowski, J. Kisielewski, E. Michalski, K. Ozga, I.V. Kityk, T. Lukasiewicz, Opt. Commun. 250 (2005) 334;
I.V. Kityk, A. Majchrowski, Opt. Mater. 26 (2004) 33.
[8] B. Teng, J. Wang, Z. Wang, H. Jiang, X. Hu, R. Song, H. Liu, Y. Liu, J. Wei, Z. Shao, J. Cryst. Growth 224 (2001) 280.
[9] Z. Wang, B. Teng, K. Fu, X. Xu, R. Song, C. Du, H. Jiang, J. Wang, Y. Liu, Z. Shao, Opt. Commun. 202 (2002) 217;
A.H. Reshak, S. Auluck, I.V. Kityk, A. Majchrowski, D. Kasprowicz, M. Drozdowski, J. Kisielewski, T. Lukasiewicz, E. Michalski, J. Mater. Sci. 41 (2006) 1927.
[10] Z. Lin, Z. Wang, C. Chen, M.H. Lee, J. Appl. Phys. 90 (2001) 5585.
[11] M. Ghotbi, Z. Sun, A. Majchrowski, E. Michalski, I.V. Kityk, Appl. Phys. Lett. 89 (2006) 173124.
[12] D. Xue, K. Betzler, H. Hesse, D. Lammers, Solid State Commun. 114 (2000) 21.
[13] J. Barbier, N. Penin, A. Denoyer, L.M.D. Cranswick, Solid State Sci. 7 (2005) 1055.
[14] Ali Hussain Reshak, I.V. Kityk, S. Auluck, J. Alloys Compds., in press, Available online 26 June 2007, doi:10.1016/j.jallcom.2007.06.070.
[15] P. Blaha, K. Schwarz, G.K.H. Madsen, D. Kvasnicka, J. luitz, WIEN2K, "An Augmented Plane Wave + Local Orbitals Program for Calculating Crystal Properties," Karlheinz Schwarz, Techn. Universitat, Wien, Austria, ISBN 3-9501031-1-2, 2001.
[16] P. Hohenberg, W. Kohn, Phys. Rev. B 136 (1964) 864.
[17] W. Kohn, L.J. Sham, Phys. Rev. A 140 (1965) 1133.
[18] O. Jepsen, O.K. Andersen, Solid State Commun. 9 (1971) 1763;
G. Lehmann, M. Taut, Phys. Stat. Sol. B 54 (1972) 496.
[19] J.A. Wilson, A.D. Yoffe, Adv. Phys. 18 (1969) 193.
[20] Ali Hussain Reshak, S. Auluck, Phys. Rev. B 68 (2003) 245113.
[21] Sangeeta Sharma, S. Auluck, M.A. Khan, Pramana J. Phys. 54 (1999) 431.
[22] B.F. Levine, Phys. Rev. B 7 (1973) 2600 and references therein.
[23] F. Nastos, B. Olejnik, K. Schwarz, J.E. Sipe, Phys. Rev. B 72 (2005) 045223.
[24] H. Tributsch, Z. Naturforsch. A 32A (1977) 972.
[25] S. Sharma, J.K. Dewhurst, C. Ambrosch-Draxl, Phys. Rev. B 67 (2003) 165332.
[26] Ali Hussain Reshak, Ph.D. Thesis, Indian Institute of Technology, Roorkee, India, 2005.
[27] D.E. Aspnes, Phys. Rev. B 6 (1972) 4648.
[28] W. Boyd, Nonlinear Optics, Academic Press, Boston, 1992.